

# Simultaneous mapping of the electric and magnetic photonic local density of states above dielectric nanostructures using rare-earth doped films

Peter R. Wiecha,<sup>1,\*</sup> Clément Majorel,<sup>1</sup> Christian Girard,<sup>1</sup> Arnaud Arbouet,<sup>1</sup> Bruno Masenelli,<sup>2</sup> Olivier Boisron,<sup>3</sup> Aurélie Lecestre,<sup>4</sup> Guilhem Larrieu,<sup>4</sup> Vincent Paillard,<sup>1</sup> and Aurélien Cuche<sup>1,†</sup>

<sup>1</sup>*CEMES, Université de Toulouse, CNRS, Toulouse, France*

<sup>2</sup>*Université de Lyon, INSA-Lyon, ECL, UCBL, CPE, CNRS, INL-UMR5270, Villeurbanne, France*

<sup>3</sup>*Université de Lyon, CNRS, ILM-UMR 5306, Villeurbanne, France*

<sup>4</sup>*LAAS, Université de Toulouse, CNRS, INP, Toulouse, France*

We propose a simple experimental technique to separately map the electric and magnetic components of the photonic local density of states (LDOS) of dielectric nanostructures, using a few nanometer thin film of rare-earth ion doped clusters. Rare-earth ions provide electric and magnetic dipole transitions of similar magnitude. By recording the photoluminescence from the deposited layer excited by a focused laser beam, we are able to simultaneously map the electric and magnetic LDOS of individual nanostructures. In spite of being a diffraction-limited far-field method with a spatial resolution of a few hundred nanometers, our approach appeals by its simplicity and high signal-to-noise ratio. We demonstrate our technique at the example of silicon nanorods and dimers, in which we find a significant separation of electric and magnetic near-field contributions. Our method paves the way towards the efficient and rapid characterization of the electric and magnetic optical response of complex photonic nanostructures.

In the last decades, photonic nanostructures emerged as powerful instruments to control light at the subwavelength scale.<sup>1</sup> The interest in nano-optics lies usually in the control of the optical *electric* field, since the response of materials to rapidly oscillating magnetic fields is extremely weak. Actually, materials with a substantial magnetic response to electromagnetic radiation (*i.e.*  $\mu \neq 1$ ) are not known in nature. However, properly designed nanostructures allow to significantly boost the magnetic response. For instance metallic (split-)ring resonators support a magnetic moment which is proportional to the area covered by the ring's aperture. For frequencies in the visible range this area is usually about  $10^6$  times larger than the equivalent area in atoms, defined by the Bohr radius, which explains the emergence of observable effects related to the optical magnetic field.<sup>2</sup> In consequence, it is possible to overcome the natural limitation to  $\mu = 1$  by designing so-called meta-materials, which are ordered arrangements of meta-units like splitting resonators.<sup>3</sup>

Using metals requires nanostructures of complex shape to obtain a significant magnetic response. On the other hand, in dielectrics of high refractive index, a magnetic response arises naturally from the curl of the electric field.<sup>4,5</sup> Very simple geometries like spheres<sup>6</sup> or cylinders<sup>7</sup> are actually sufficient to induce a strong magnetic field enhancement.<sup>8</sup> An additional advantage of many high-index dielectrics is their low dissipation compared to metals.<sup>9</sup> Silicon (Si) for example has a very low absorption through the entire visible range. This weak absorption associated to the indirect gap in the near infrared becomes cumbersome only for applications involving propagation of visible light across distances of tens to hundreds

of microns. Thus, in small dielectric nano-structures the absorption can usually be neglected.<sup>10</sup> In summary, high-index dielectric nanostructures seem to be an appropriate platform to study the confinement of optical electric and magnetic fields. Most importantly, it has been shown that the electric and magnetic fields are located in different regions around dielectric nanostructures. In other words, the electric and magnetic parts of the photonic local density of states (LDOS) can be spatially separated around subwavelength small particles.<sup>11</sup>

The separation of magnetic and electric field energy close to photonic nano-structures was first demonstrated by measuring the local magnetic field intensity using scanning near-field optical microscopy (SNOM). The sensitivity to the magnetic part of the optical near-field is provided by particular SNOM-tips, coated with nanoscale metal rings or split-ring resonators.<sup>12–15</sup> Another possibility to access the LDOS is to use optical quantum transitions as near-field probe and exploit the proportionality of the LDOS to the decay rate of a quantum emitter.<sup>16–19</sup> However, in order to discriminate between electric and magnetic LDOS, probes supporting both electric and magnetic dipole transitions need to be used. This drastically limits the range of possible emitters: Electric dipole (ED) transitions are usually 4–5 orders of magnitude stronger than magnetic dipole (MD) transitions.<sup>20</sup> Still, intense MD transitions can be found occasionally, for instance in lanthanoid ions (also known as rare earth elements), such as europium ( $\text{Eu}^{3+}$ ),<sup>21</sup> which have recently been suggested as probes for the detection of the optical magnetic field.<sup>22</sup> A peculiarity of  $\text{Eu}^{3+}$  is that electric and magnetic dipole transitions of comparable strength occur at close wavelengths. Both start from the  $^5D_0$  energy level via deexcitation to the  $^7F_2$  (ED) and the  $^7F_1$  level (MD).<sup>23</sup> Those transitions lie in the visible, around  $\lambda_{\text{ED}} \approx 610$  nm and  $\lambda_{\text{MD}} \approx 590$  nm.<sup>22</sup> This renders europium ions particu-

\* e-mail : [peter.wiecha@cemes.fr](mailto:peter.wiecha@cemes.fr)

† e-mail : [cuche@cemes.fr](mailto:cuche@cemes.fr)

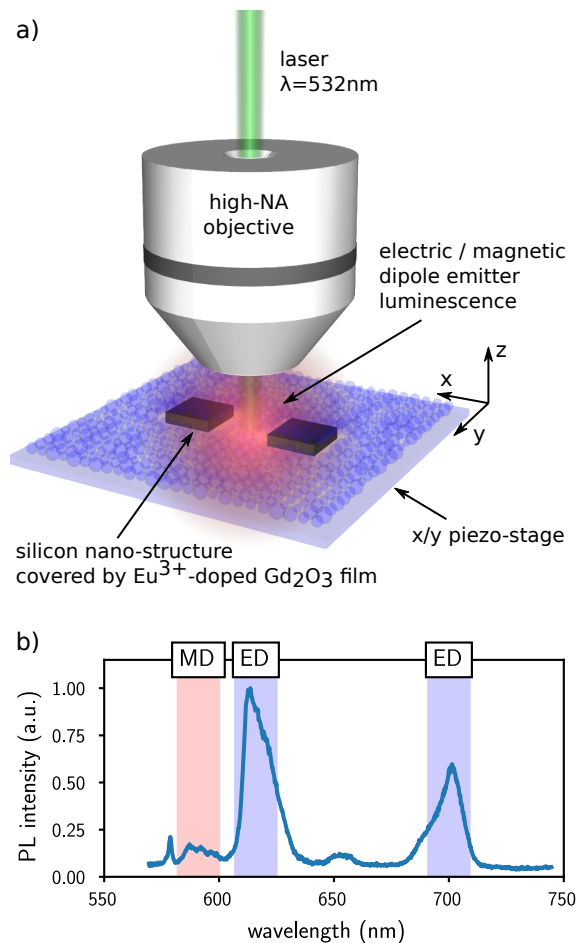


FIG. 1. a) Sketch of the experimental setup. A tightly focused laser beam (NA 0.9,  $\lambda = 532$  nm) is raster-scanned over a high-index dielectric nano-structure (in our case: silicon). An  $\text{Eu}^{3+}$ -doped  $\text{Gd}_2\text{O}_3$  film is deposited on the structure. The photoluminescence due to the magnetic and electric dipole transitions of the europium ions is collected in back-scattering by the microscope objective and analyzed with a spectrometer at each raster-scan position. b) Example spectrum of the photoluminescence from the  $\text{Eu}^{3+}$ -ion. Emission due to magnetic dipole (MD) and electric dipole (ED) transitions are underlined by red and blue color, respectively.

larly promising as potential probes for the electric and magnetic LDOS around dielectric nanostructures: despite their similar transition energies, the ED and MD transitions are spectrally separated enough to easily distinguish them *e.g.* using simple color-filters.

Thanks to their unique properties, rare-earth ion doped media have been used as probes to determine the relative intensities of electric and magnetic LDOS at fixed positions or on non-structured samples like interfaces.<sup>24–26</sup> By attaching an  $\text{Eu}^{3+}$  doped nano-crystal to a SNOM tip, the 3D spatial distribution of the electric and magnetic LDOS on top of gold strips has been recorded.<sup>17</sup> The methods employed in these studies were however limited, either with respect to the lack of spa-

tial resolution or, in the case of emitter-doped SNOM tips, require complex experimental setups.<sup>17,27</sup> SNOM-techniques furthermore suffer from a poor signal to noise ratio due to the low number of quantum emitters at the scanning tip.

In this letter, we propose an alternative approach: we deposit a nanometric thin film of  $\text{Eu}^{3+}$ -doped nano-clusters on high-index dielectric nanostructures and raster-scan the sample under a tightly focused laser beam. In this configuration, the laser beam is taking the role of the SNOM-tip. In consequence, the spatial resolution is limited by diffraction but currently available SNOM techniques are neither able to provide much better resolution due to the large size of the rare-earth doped nanocrystals at the tips, required to yield detectable signals (values around 200 – 300 nm were reported<sup>17</sup>). In the following, we report experimental maps of the luminescence from either the electric or magnetic dipole transitions. These results show the good signal to noise ratio and spatial resolution obtained with a rather simple approach. We also compare our experimental results with computed maps of the electric and magnetic LDOS.

## I. PHOTOLUMINESCENCE FROM $\text{Eu}^{3+}$ -DOPED NANOCLUSTER FILM DEPOSITED ON SILICON NANOSTRUCTURES

### Sample preparation

Our sample contains silicon dimers consisting of two elements, each  $300 \times 300 \times 90 \text{ nm}^3$  ( $L \times W \times H$ ) large, separated by a gap  $G$  of variable size. These nanostructures are fabricated in a top-down approach, where a single layer of negative-tone resist, namely hydrogen silsesquioxane (HSQ), is patterned by electron-beam lithography.<sup>28</sup> Subsequent reactive ion etching in the  $H = 90 \text{ nm}$  Si overlayer of commercial silicon on insulator (SOI) substrates defines the structures. The remaining HSQ-layer on the top of the structures induces an additional  $\text{SiO}_2$  capping of approximately 20 nm. This layer acts as a spacer between the nanostructures and the  $\text{Eu}^{3+}$  doped film. For more details on the fabrication process, see Ref. 29. After the lithography, a 30 nm thick film of  $\text{Eu}^{3+}$ -doped  $\text{Gd}_2\text{O}_3$  nano-clusters is deposited. The film is synthesized by the Low Energy Cluster Beam Deposition (LECBD) technique. LECBD consists in the ablation of a solid  $\text{Gd}_2\text{O}_3$  pellet, doped at 7% with europium, *via* a pulsed Nd:YAG laser (10 ns pulse width). The ablated fragments are then broken into small clusters, first by the injection of He (20 mbar) as a buffer gas in the nucleation chamber and subsequently during its adiabatic expansion through a micrometer nozzle. The resulting nanocrystals are deposited on the dielectric nanostructures without further breaking (“soft landing”). More details about the process and the resulting nanocrystals can be found in Refs. 27 and 30.

## Experimental configuration

Our experimental setup consists of a confocal microscope, equipped for Raman spectroscopy. A simplified sketch of the experiment is shown in figure 1a. A linearly polarized cw laser at  $\lambda = 532$  nm is focused by a  $\times 100$  air objective (NA = 0.9) on the sample, which lies on a  $XY$  piezo stage. The photoluminescence (PL) from the sample is collected by the same microscope objective. The PL is dispersed by a grating (300 grooves per mm) and detected by a CCD camera (Andor iDus 401), with an integration time of  $t_{\text{exposure}} = 2$  s. A typical spectrum from the  $\text{Eu}^{3+}$ -doped  $\text{Gd}_2\text{O}_3$  film is shown in figure 1b. Finally, we obtain 2D PL maps by raster-scanning the sample under the laser with the piezo-stage. At each position, we acquire a spectrum and extract the emission intensities from the spectral ranges corresponding to magnetic or electric transitions ( $\lambda = (590 \pm 10)$  nm, respectively  $\lambda = (610 \pm 10)$  nm) during post-processing. The signal is normalized to the background PL intensity, recorded far from the nanostructures.

## Experimental results

The laser polarization was arbitrarily chosen perpendicular to the long axis of the dimers. A laser polarization parallel or perpendicular to the dimers yields almost identical results (see supporting informations (SI)). This is a surprising finding because in the vicinity of the nanodimers, the spatial near-field distribution depends significantly on the laser polarization (see also SI). Thus, since the PL-mappings are independent of the laser polarization, we conclude that we excite the  $\text{Eu}^{3+}$  ions close to saturation – keeping in mind that the ED and MD transitions in  $\text{Eu}^{3+}$  are both populated by excitation of the  $^5\text{D}_1$  level *via* the local *electric* field.<sup>23</sup> This assumption is also supported by a measurement of the PL intensity of the bare  $\text{Eu}^{3+}$  film, as function of the laser-power, where a plateau in the PL intensity appears for similar values of the excitation field intensity (see SI). In this regime, the observed variations in the ED (resp. MD) photoluminescence maps are independent of the optical excitation and only driven by the electric (resp. magnetic) LDOS at the *emission* wavelength. This conclusion is in agreement with a recent study of the directional emission of  $\text{Eu}^{3+}$  ions, coupled to plasmonic nanostructures. In the latter, the most significant modification of the  $\text{Eu}^{3+}$ -PL is ascribed to the improved light out-coupling, whereas the plasmonic enhancement of the excitation has only a weak impact on the emission.<sup>31</sup>

Raster-scan maps, measured on silicon dimers with gap-sizes between 0 nm and 300 nm, are shown in figure 2b. Sketches and scanning electron microscopy (SEM) images of the corresponding structures are shown in Fig. 2a. In the experimental maps, a clear inversion of the contrast between emission from MD and ED transitions is observed. The MD photoluminescence yields

a maximum intensity when the laser-beam is focused on the structure. The ED emission maps on the other hand consistently contain valley-like features, where a reduction in intensity is surrounded by a stronger PL. A single nano-rod (figure 2i) yields one peak (MD) or one valley feature (ED). However, as soon as a gap is introduced (figures 2ii-iv), the maps start to change significantly. The magnetic dipole emission yields confined hot-spots at the silicon block positions, whereas the PL maps from the ED transition show hot-spots outside the dimer, located above and below the gap. The ED maps show furthermore circular features around the two silicon blocks, each with a minimum PL intensity in the center.

We conclude that the ED and MD maps recorded with our technique should reflect the electric, respectively magnetic LDOS at the location of the  $\text{Eu}^{3+}$ -film. We will confirm this assumption in the following using numerical simulations.

## II. CALCULATING THE ELECTRIC AND MAGNETIC LDOS

To confirm that our technique allows the simultaneous recording of the electric and magnetic LDOS, we compare the experimental data to calculated LDOS maps.

### Decay-rate of electric/magnetic emitters

The decay-rate enhancement of a quantum emitter is proportional to the partial LDOS at the emitter's location.<sup>18,32</sup> With “partial” LDOS, we refer to the projection of the LDOS onto a specific direction (dipole orientation) and to the nature of the dipole transition (electric or magnetic). The full LDOS can be obtained by averaging over all possible dipole orientations. Hence, the computation of the decay-rate modification of electric and magnetic dipole transitions also yields the photonic local density of states.

The decay-rate of electric or magnetic dipolar transitions is modified by the presence of a polarizable material. The effect is intuitively understandable for an electric dipole transition  $\mathbf{p}$ , as a result of the enhancement (or weakening) of the electric near-field due to the dielectric contrast or optical resonances, and the back-action of the radiated field on the dipole emitter. It is possible to derive an integral equation describing the decay-rate  $\Gamma_e$  of an electric dipole transition at a position  $\mathbf{r}_0$ , close to an arbitrary nano-structure.<sup>11,18</sup>

$$\Gamma_e(\mathbf{r}_0, \omega) = \Gamma_e^0(\omega) \times \left( 1 + \frac{3}{2k_0^3} \mathbf{u} \cdot \text{Im}(\mathcal{S}_p^{\text{EE}}(\mathbf{r}_0, \mathbf{r}_0, \omega)) \cdot \mathbf{u} \right), \quad (1)$$

In this equation,  $\Gamma_e^0(\omega) = 4k_0^3 p^2 / 3\hbar$  is the decay rate of the emitter in the absence of a structure with the vacuum

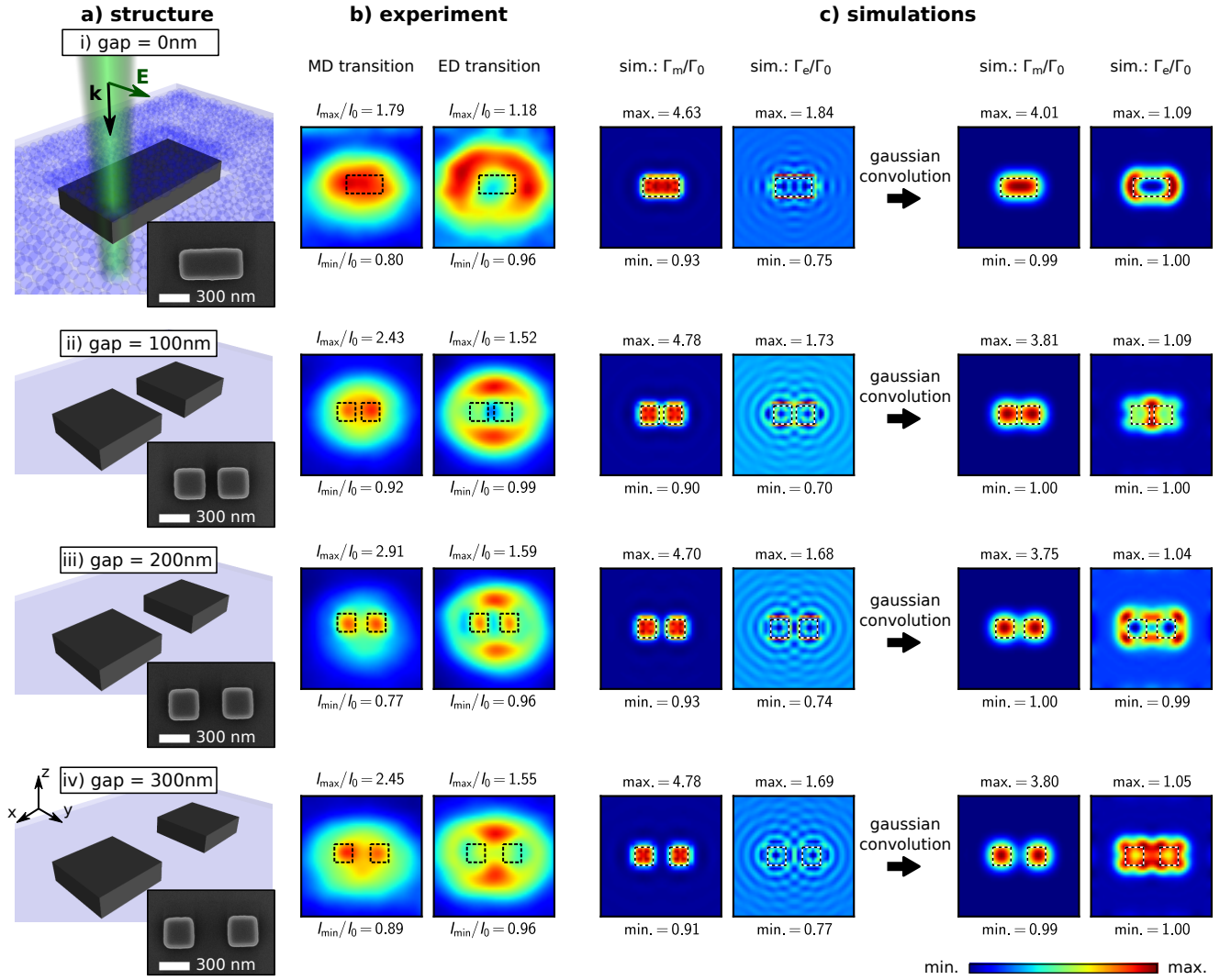


FIG. 2. Comparison of the experimental results with simulated decay-rate maps for different gap sizes i)  $G = 0$  nm, ii)  $G = 100$  nm, iii)  $G = 200$  nm and iv)  $G = 300$  nm. a) Sketches and SEM images of the corresponding structures. SEM images were taken prior to  $\text{Eu}^{3+}$ -cluster deposition. Scale bars are 300 nm. b) Experimental results recorded with an incident polarization along the dimer axis. Left column: MD transition, right column: ED transition. c) Simulated decay-rate maps before (left columns) and after convolution with a Gaussian profile (right columns). The subplots on the left show the magnetic dipole in-plane decay rates  $\Gamma_m^{xy}$ , the subplots on the right the respective ED maps  $\Gamma_e^{xy}$ . The waist of the Gaussian profile is  $\eta = 200$  nm. All color-maps show areas of  $2 \times 2 \mu\text{m}^2$ , dashed lines indicate the positions of the silicon dimer.

wavenumber  $k_0$ .  $\mathbf{u}$  and  $p$  denote the dipole orientation and amplitude, respectively, and

$$\mathcal{S}_p^{\text{EE}}(\mathbf{r}, \mathbf{r}_0, \omega) = \int_V d\mathbf{r}' \int_V d\mathbf{r}'' \chi(\mathbf{r}', \omega) \mathbf{G}^{\text{EE}}(\mathbf{r}, \mathbf{r}', \omega) \cdot \mathbf{K}(\mathbf{r}', \mathbf{r}'', \omega) \cdot \mathbf{G}^{\text{EE}}(\mathbf{r}'', \mathbf{r}_0, \omega). \quad (2)$$

$\mathbf{K}$  is the generalized propagator (see *e.g.* Ref. 33). The propagator  $\mathbf{G}^{\text{EE}}$  can be found by identification using the electric field emitted by a dipolar source<sup>34</sup> and the Green's Dyad for vacuum<sup>33</sup> (*c.f.* also Ref. 11).

Eq. (1) describes the decay-rate of an *electric* quantum emitter. It turns out, that although no known mate-

rial has a direct response to rapidly oscillating magnetic fields, the decay rate of a magnetic dipole transition is nevertheless influenced by the presence of material. Such *magnetic-magnetic* response function associated with a structure which, by itself, has no direct magnetic response, arises from the *electric* field emitted by the magnetic dipole, which can interact with the environment. In particular, Mie-type optical resonances in dielectric nanostructures often induce curled features in the electric near-field spatial distribution, leading to a strong enhancement of the magnetic field via the Maxwell's equation  $ik_0 \mathbf{B}(\mathbf{r}) = \text{rot} \mathbf{E}(\mathbf{r})$  (for monochromatic fields,  $k_0 = 2\pi/\lambda_0$ ). Formally, the magnetic decay-rate in the

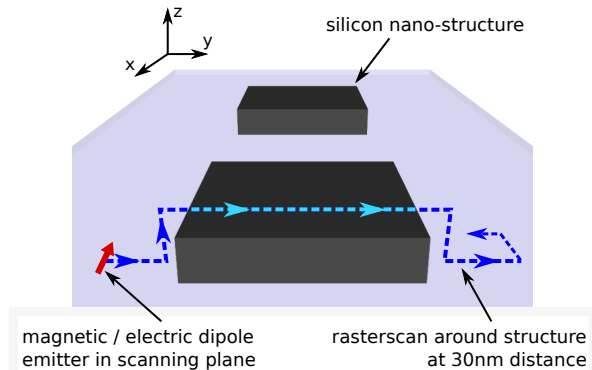


FIG. 3. Sketch of the simulation procedure. A magnetic or electric dipolar emitter is raster-scanned across the nano-structure at 30 nm above its surface, simulating the distance of the doped film to the top surface of the structures (20 nm SiO<sub>2</sub> spacing layer). Far from the structure, the scan-height is at 30 nm above the ground-level. The raster-scan is repeated for emitter orientations along  $Ox$  and  $Oy$ , the decay-rates are averaged.

vicinity of arbitrary nanostructures can be calculated in complete analogy to equation (1) by replacing the tensors  $\mathbf{G}^{\text{EE}}$  in equation (2) with the Dyads  $\mathbf{G}^{\text{HE}}$  (first occurrence) and  $\mathbf{G}^{\text{EH}}$  (second occurrence, *c.f.* reference 11). The latter tensors are often called “mixed-field susceptibilities”.<sup>35–37</sup>

### Simulation of raster-scan maps

To solve Eq. (1) numerically, the integrals in Eq. (2) can be converted to discrete sums over the mesh-points of a volume-discretized nanostructure. To calculate raster-scans of the MD and ED decay-rates (hence maps of the electric and magnetic LDOS), we make use of the concept of a generalized propagator.<sup>33</sup> This approach significantly speeds up the computation of the decay-rate at multiple locations, as explained in reference 38.

The specific simulation procedure is illustrated in figure 3. We raster-scan a dipolar emitter of either magnetic ( $\Gamma_m$ ,  $\lambda_{\text{MD}} = 590$  nm) or electric nature ( $\Gamma_e$ ,  $\lambda_{\text{ED}} = 610$  nm) across a discretized nano-dimer (discretization step  $s = 20$  nm). The dimer lies in a homogeneous environment of refractive index  $n_{\text{env}} = 1.8$ , corresponding to the optical index of the Gd<sub>2</sub>O<sub>3</sub> film.<sup>39</sup> For an analysis of the impact of the environment refractive index, see also SI. The distance between emitter and structure is kept at 30 nm. Far from the structure, the dipole is scanned at 30 nm above the substrate. In this way, we account for the distance between the Eu<sup>3+</sup>-cluster film and the nanostructures due to the 20 nm thick SiO<sub>2</sub> layer (for an analysis of the emitter-structure distance, see SI). We neglect dipole emitters oriented along  $Oz$ , because their emission, a toroidal radiation pattern propagating per-

pendicular to the  $Z$ -axis, is not detected in our experimental configuration (see also SI). Therefore, the simulated maps only take into account dipoles located in a plane parallel to the substrate (the computed values being the average of the contributions of dipoles oriented along  $Ox$  and  $Oy$ ). We denote these average decay rates  $\Gamma_m^{xy}$  and  $\Gamma_e^{xy}$  for MD and ED, respectively.

The direct result of this procedure has a far too high spatial resolution (see the two columns on the left of figure 2c). Therefore, to account for the diffraction limited size of the laser-spot, we convolve the simulated mapping with a Gaussian profile of waist  $\eta = 200$  nm. Our numerical signal power is described by the following equation:

$$I_{\text{signal}}(\mathbf{r}) = \int_{A_{\text{spot}}} \hbar\omega_0 n(\mathbf{r}') \Gamma_i^{xy}(\mathbf{r}') \exp\left(-\frac{\mathbf{r}'^2}{2\eta^2}\right) d\mathbf{r}'. \quad (3)$$

The integral runs over the area of the laser-spot  $A_{\text{spot}}$ ,  $\hbar\omega_0$  is the photon energy of the MD or ED transition,  $n$  is the density of emitting Eu<sup>3+</sup> ions (which we consider homogeneous).  $\Gamma_i^{xy}$  is the  $x$ - $y$ -averaged decay rate of either a magnetic ( $i = “m”$ ) or an electric ( $i = “e”$ ) dipole transition. The exponential factor accounts for the Gaussian intensity profile of the laser beam. The simulated maps after convolution are shown in the right columns of Fig. 2c. We note that a similar procedure has been successfully used to recover the near-field intensity distribution from two-photon luminescence (TPL) measurements on plasmonic nanostructures.<sup>40</sup>

### Discussion

Comparing the simulated and experimental results in figure 2, we observe that the features in the simulated maps are more confined around the dimer blocks. Nevertheless the general agreement is good, the global features and trends observed in the experimental maps are reproduced by the simulations. Also the quantitative trends in the intensity ratios are correctly recovered by the simulations.

Compared to the simulations, the experimental results are less sharp and possess broader features. This can be explained by the approximative nature of our numerical approach. First, we only take into account a single point-emitter, raster-scanned across the silicon dimer. In the experiment on the other hand, a large collection of emitters is excited simultaneously at each raster-scan position. Furthermore, the emitters at the edge of the laser focal spot are excited with a weaker field amplitude, hence the assumption of saturated emitters is not correct in this case. Finally, in addition to the decay rate, the emission pattern of the dipoles may be influenced by the presence of the nanostructure,<sup>41</sup> which is not taken into account in our simplified model.

A better agreement could probably be achieved by simulating an actual “layer” of dipoles, instead of raster-scanning a single emitter, and by taking into account the

modified radiation pattern due to the inhomogeneous environment. However, this would require to consider the excitation intensity as function of the emitter position with respect to the center of the focal spot. The assumption of saturated emitters would in general no longer be valid. A possible approach to this problem could be the description of the  $\text{Eu}^{3+}$  emitters in the layer as non-saturated three-level molecules.<sup>42,43</sup> These more sophisticated theoretical approaches lie outside the scope of this study and will be the subject of a future work.

### III. CONCLUSION

In conclusion, we presented a technique allowing the parallel mapping of the electric and magnetic components of the LDOS above dielectric nanostructures via a far-field detection scheme. To this end, a nanometer thin film of rare-earth ion doped clusters is deposited on top of the structures and excited by a tightly focused laser beam. The laser beam is raster-scanned across the structures to obtain 2D maps of the LDOS. The emission from either electric or magnetic dipole transitions is extracted from the photoluminescence measurements, yielding the corresponding contributions to the local density of photonic states. Numerical simulations of the electric and magnetic LDOS are in good agreement with the experimental results. These results show that the electric and magnetic near-field intensity is confined in distinct regions around simple dielectric nanostructures such as

rods or dimers. The observed contrast of the electric LDOS is furthermore in agreement with results of a recently proposed technique, for spectrally resolved mapping of the electric LDOS.<sup>44</sup>

Despite being a far-field technique, we want to point out that the spatial resolution is comparable to similar proposed methods which use a SNOM-like setup.<sup>17,44</sup> The resolution can be improved using an oil immersion objective and further increased to a deeply sub-wavelength regime in a TERS-like setup, using the near-field enhancement at a plasmonic tip to excite very small volumes of the emitter-doped film. A refined numerical model including non-saturated excitation and a two-dimensional distribution of the emitters might help to improve the agreement of the predictions with the experimental mappings. Our work paves the way towards the very rapid and simple experimental characterization of the response of photonic nanostructures to both, the electric and magnetic field of visible light.

### ACKNOWLEDGMENTS

This work was supported by Programme Investissements d’Avenir under the program ANR-11-IDEX-0002-02, reference ANR-10-LABX-0037-NEXT, by the LAAS-CNRS micro and nanotechnologies platform, a member of the French RENATECH network and by the computing facility center CALMIP of the University of Toulouse under grant P12167.

- 
- <sup>1</sup> L. Novotny and B. Hecht, *Principles of Nano-Optics* (Cambridge University Press, Cambridge ; New York, 2006).
- <sup>2</sup> H. Giessen and R. Vogelgesang, *Science* **326**, 529 (2009).
- <sup>3</sup> J. B. Pendry, *Physical Review Letters* **85**, 3966 (2000).
- <sup>4</sup> R. Merlin, *Proceedings of the National Academy of Sciences* **106**, 1693 (2009).
- <sup>5</sup> A. I. Kuznetsov, A. E. Miroshnichenko, Y. H. Fu, J. Zhang, and B. Luk’yanchuk, *Scientific Reports* **2**, 492 (2012).
- <sup>6</sup> A. B. Evlyukhin, S. M. Novikov, U. Zywietz, R. L. Eriksen, C. Reinhardt, S. I. Bozhevolnyi, and B. N. Chichkov, *Nano Letters* **12**, 3749 (2012).
- <sup>7</sup> P. Kapitanova, V. Ternovski, A. Miroshnichenko, N. Pavlov, P. Belov, Y. Kivshar, and M. Tribelsky, *Scientific Reports* **7**, 731 (2017).
- <sup>8</sup> A. I. Kuznetsov, A. E. Miroshnichenko, M. L. Brongersma, Y. S. Kivshar, and B. Luk’yanchuk, *Science* **354** (2016), 10.1126/science.aag2472.
- <sup>9</sup> P. Albella, R. Alcaraz de la Osa, F. Moreno, and S. A. Maier, *ACS Photonics* **1**, 524 (2014).
- <sup>10</sup> P. Albella, M. A. Poyli, M. K. Schmidt, S. A. Maier, F. Moreno, J. J. Sáenz, and J. Aizpurua, *The Journal of Physical Chemistry C* **117**, 13573 (2013).
- <sup>11</sup> P. R. Wiecha, A. Arbouet, A. Cuche, V. Paillard, and C. Girard, arXiv:1707.07006 [cond-mat, physics:physics] (2017), arXiv:1707.07006 [cond-mat, physics:physics].
- <sup>12</sup> E. Devaux, A. Dereux, E. Bourillot, J.-C. Weeber, Y. Lacroute, J.-P. Goudonnet, and C. Girard, *Applied Surface Science* **164**, 124 (2000).
- <sup>13</sup> E. Devaux, A. Dereux, E. Bourillot, J.-C. Weeber, Y. Lacroute, J.-P. Goudonnet, and C. Girard, *Physical Review B* **62**, 10504 (2000).
- <sup>14</sup> M. Burreli, D. van Oosten, T. Kampfrath, H. Schoenmaker, R. Heideman, A. Leinse, and L. Kuipers, *Science* **326**, 550 (2009).
- <sup>15</sup> I. V. Kabakova, A. de Hoogh, R. E. C. van der Wel, M. Wulf, B. le Feber, and L. Kuipers, *Scientific Reports* **6** (2016), 10.1038/srep22665.
- <sup>16</sup> C. Girard, T. David, C. Chicanne, A. Mary, G. C. des Francs, E. Bourillot, J.-C. Weeber, and A. Dereux, *Europhysics Letters (EPL)* **68**, 797 (2004).
- <sup>17</sup> L. Aigouy, A. Cazé, P. Gredin, M. Mortier, and R. Carminati, *Physical Review Letters* **113**, 076101 (2014).
- <sup>18</sup> R. Carminati, A. Cazé, D. Cao, F. Peragut, V. Krachmalnicoff, R. Pierrat, and Y. De Wilde, *Surface Science Reports* **70**, 1 (2015).
- <sup>19</sup> A. Cuche, M. Berthel, U. Kumar, G. Colas des Francs, S. Huant, E. Dujardin, C. Girard, and A. Drezet, *Physical Review B* **95**, 121402 (2017).
- <sup>20</sup> T. H. Taminiau, S. Karaveli, N. F. van Hulst, and R. Zia, *Nature Communications* **3**, ncomms1984 (2012).
- <sup>21</sup> W. T. Carnall, P. R. Fields, and K. Rajnak, *The Journal of Chemical Physics* **49**, 4412 (1968).
- <sup>22</sup> N. Noginova, G. Zhu, M. Mavy, and M. A. Noginov, *Journal of Applied Physics* **103**, 07E901 (2008).

- <sup>23</sup> D. G. Baranov, R. S. Savelev, S. V. Li, A. E. Krasnok, and A. Alù, *Laser & Photonics Reviews* **11**, 1600268 (2017).
- <sup>24</sup> S. Karaveli and R. Zia, *Physical Review Letters* **106**, 193004 (2011).
- <sup>25</sup> R. Hussain, D. Keene, N. Noginova, and M. Durach, *Optics Express* **22**, 7744 (2014).
- <sup>26</sup> B. Choi, M. Iwanaga, Y. Sugimoto, K. Sakoda, and H. T. Miyazaki, *Nano Letters* **16**, 5191 (2016).
- <sup>27</sup> A. Cuche, B. Masenelli, G. Ledoux, D. Amans, C. Dujardin, Y. Sonnefraud, P. Mélinon, and S. Huant, *Nanotechnology* **20**, 015603 (2009).
- <sup>28</sup> Y. Guerfi, F. Carcenac, and G. Larrieu, *Microelectronic Engineering* **110**, 173 (2013).
- <sup>29</sup> P. R. Wiecha, A. Arbouet, C. Girard, A. Lecestre, G. Larrieu, and V. Paillard, *Nature Nanotechnology* **12**, 163 (2017).
- <sup>30</sup> A. Perez, P. Melinon, V. Dupuis, L. Bardotti, B. Masenelli, F. Tournus, B. Prevel, J. Tuillon-Combes, E. Bernstein, A. Tamion, N. Blanc, D. Tainoff, O. Boisron, G. Guiraud, M. Broyer, M. Pellarin, N. Fatti, F. Vallee, E. Cottancin, J. Lerne, J.-L. Vialle, C. Bonnet, P. Maioli, A. Crut, C. Clavier, J. Rousset, and F. Morfin, *International Journal of Nanotechnology* **7**, 523 (2010).
- <sup>31</sup> S. Murai, M. Saito, H. Sakamoto, M. Yamamoto, R. Kamakura, T. Nakanishi, K. Fujita, M. A. Verschuuren, Y. Hasegawa, and K. Tanaka, *APL Photonics* **2**, 026104 (2017).
- <sup>32</sup> P. Lunnemann and A. F. Koenderink, *Scientific Reports* **6**, srep20655 (2016).
- <sup>33</sup> O. J. F. Martin, C. Girard, and A. Dereux, *Physical Review Letters* **74**, 526 (1995).
- <sup>34</sup> G. S. Agarwal, *Physical Review A* **11**, 230 (1975).
- <sup>35</sup> C. Girard, J.-C. Weeber, A. Dereux, O. J. F. Martin, and J.-P. Goudonnet, *Physical Review B* **55**, 16487 (1997).
- <sup>36</sup> U. Schröter, *The European Physical Journal B* **33**, 297 (2003).
- <sup>37</sup> I. Sersic, C. Tuambilangana, T. Kampfrath, and A. F. Koenderink, *Physical Review B* **83**, 245102 (2011).
- <sup>38</sup> A. Teulle, R. Marty, S. Viarbitskaya, A. Arbouet, E. Dujardin, C. Girard, and G. Colas des Francs, *Journal of the Optical Society of America B* **29**, 2431 (2012).
- <sup>39</sup> A. A. Dakhel, *Journal of Optics A: Pure and Applied Optics* **3**, 452 (2001).
- <sup>40</sup> P. Ghenuche, S. Cherukulappurath, T. H. Taminiau, N. F. van Hulst, and R. Quidant, *Physical Review Letters* **101**, 116805 (2008).
- <sup>41</sup> A. G. Curto, T. H. Taminiau, G. Volpe, M. P. Kreuzer, R. Quidant, and N. F. van Hulst, *Nature Communications* **4**, 1750 (2013).
- <sup>42</sup> C. Girard, O. J. F. Martin, G. Lévêque, G. C. des Francs, and A. Dereux, *Chemical Physics Letters* **404**, 44 (2005).
- <sup>43</sup> G. Colas des Francs, C. Girard, T. Laroche, G. Lévêque, and O. J. F. Martin, *The Journal of Chemical Physics* **127**, 034701 (2007).
- <sup>44</sup> S. V. Makarov, I. S. Sinev, V. A. Milichko, F. E. Komissarenko, D. A. Zuev, E. V. Ushakova, I. S. Mukhin, Y. F. Yu, A. I. Kuznetsov, P. A. Belov, I. V. Iorsh, A. N. Poddubny, A. K. Samusev, and Y. S. Kivshar, *Nano Letters* **18**, 535 (2018).